ANALYSIS OF UNSTEADY FREE CONVECTION OVER A VERTICAL PLATE FOR KEROSENE-BASED NANOFLUID

P. LOGANATHAN and S. SANGEETHA
Department of Mathematics, Anna University, Chennai-600025, Tamilnadu, India.
logu@annauniv.edu

Abstract*— The application of nanofluids in the manufacturing industry is their ability to transfer heat rapidly between surfaces. The demand for modern technology prompts scientists to develop novel concepts and techniques for studying a material's thermophysical behavior, even though there is research on water-based nanofluids. Studying the thermal conductivity of kerosene-based nanofluids takes the convection effect into account. The purpose of this paper is to present novel numerical analysis of the two-dimensional flow of kerosene-based nanofluid past an isothermal vertical plate. At the beginning the temperature and concentration remains the same as ambient conditions. Further, changes are encountered only when the time increases. A set of unsteady, nonlinear governing equations are derived, namely, the momentum, energy, continuity, and concentration equations. The Crank-Nicolson implicit finite difference scheme is used to solve the governing equations. It is unconditionally stable. The fluid used in this contains copper nanoparticles with kerosene as the base fluid. Based on different values of physical parameters, the velocity, temperature, and concentration profiles across the boundary layer are depicted. Also, the graphs of heat transfer, mass transfer and skin friction are illustrated. With an increasing value of the Prandtl number of kerosene-based nanofluid the local skin friction coefficient decreases while the Nusselt number increases. Furthermore, the Sherwood number decreases as the Prandtl number increases. The results obtained from the study are compared with already existing results. This discloses the great correlation between current and preceding results of literature.

***Keywords*— Kerosene based nanofluid, Natural Convection, Finite difference scheme, heat and mass transfer.**

I. INTRODUCTION

Many researchers have focused on developments in the field of heat transport phenomena in recent years. The shape and size of the product are heavily influenced by the cooling of the system because of the wide variety of applications in industries and engineering for the production of electronics. Researchers found using conventional fluids for the same procedure was less effective. The young ignited mind therefore developed a new mix of nanoparticles and conventional liquids. Nanoparticles have a higher conductivity than conventional fluids, which enables better heat transfer. Researchers have proposed that metal oxides and carbides can transport heat through nanofluids embedded in water, kerosene, and, most likely, engine oil, ethyl glycol, etc.

Porous media are quite common in nature, so liquids flowing through them have a great deal of significance. Scientists and engineers have taken note of these motions due to their numerous applications in many disciplines. Thermal instability in a porous medium layer saturated by nanofluid is conveyed by Nield and Kuznetsov (2009). Kasaeian *et al*. (2017) investigated the flow and heat transfer of Nanofluids in porous media, for heat transfer enhancement purposes in thermal systems with different structures and boundary conditions. The first paper to examine stretching sheet in nanofluids of laminar flow using a model that considers Brownian motion and thermophoresis was found by Khan and Pop (2010). Hassani *et al*. (2011) presented an analytical solution using Homotopy Analysis for the boundary layer flow of a nanofluid past a stretching sheet. Acharya *et al*. (2016) investigated the convective transport in Cu-water and Cu-Kerosene nanofluid in the presence of a magnetic field between parallel plates. They solved problem by using the 4-th order RK method, equations are transformed using the similarity transformation and solved numerically. A relatively new analytical technique was also applied, namely, differential transformation method (DMT). The graphs show the characteristics of flow. The similar numerical approach was used by Narayana *et al*. (2017) to analyze thermal radiation effects on an unsteady nanofluid flow over a stretching sheet with a non-uniform heat source/sink.

In the presence of thermal radiation and a magnetic field, Reddy *et al*. (2016) investigated MHD boundary layer flow with nanofluid heat transfer over a nonlinear stretching sheet. Keller Box method is a highly popular method for solving boundary layer equations in fluid mechanics. This approach uses finite difference technologies to solve the transformed nonlinear equations numerically. The Laplace transform works best when time intervals are impulsive or uneven. In the presence of radiative heat energy, studied the MHD flow of copper-kerosene nanofluid over a vertical plate. Analyzing the transformed equations is accomplished by using the Laplace transform. Saritha and Palaniammal (2018) studied an MHD viscous nanofluid flow with thermal radiation and viscous dissipation in the presence of a gradient-dependent heat sink and found that kerosene-based nanofluids possess higher heat transfer rates than water-based nanofluids. Noghrehabadi *et al*. (2014) explored the effects of variable viscosity and thermal conductivity on the natural convection heat transfer over a vertical plate embedded in a porous medium saturated by a nanofluid are investigated.

Mutuku-Njane and Makinde (2014) examined a nanofluid containing copper *(Cu)*, Aluminium oxide *(Al_2O_3)*, and titanium dioxide *(TiO_2)* on porous vertical wall plates and convectively heated with variable suction. The numerical algorithm based on Runge-Kutta-Fehlberg integration was used to solve the boundary value problem. The free convection flow of different shapes of nanoparticles has been studied by Sobamowo (2019). The different shapes were lamina, platelets, cylindrical bricks, and sphere-shaped particles at both low and high Prandtl numbers. The solution is found by solving the coupled nonlinear equations using the differential transformation method-Pade approximant technique.

Bhatti *et al.* (2022a) modify Darcy-Brinkman-Forchheimer's model by incorporating viscous dissipation and Joule heating effects using homotopy perturbation. A multi-step differential transform method is used to obtain analytical solutions for Eyring-Powell fluid flow between two micro-parallel plates investigated by Bhatti *et al.* (2022b). A steady laminar boundary layer flow over a moving plate in a moving fluid was studied by (Ishak, et al., 2011). Fluids and plates move in opposite directions, resulting in dual solutions. Rashidi *et al.* (2022) Suggest that modifying the thermo-physical properties of fluids would lead to a decrease in entropy generation and an increase in energy efficiency. Daniel *et al.* (2022) found numerical solution by employing Keller box method to solve Electric Field Flow on Nanofluid over Stretchable Surface.

All of the studies described above resulted in a lack of scientific scrutiny of the unsteady natural convection flow of a viscous, incompressible kerosene-based nanofluid over a vertical surface. Nanofluids derived from kerosene exhibit special rheological properties, allowing them to behave differently depending on their volume concentrations. In addition, kerosene as a more suitable heat transfer fluid in industries not investigated sufficiently as to be considered for nanofluid preparation. This work aims to understand the convection heat transfer in kerosene-based nanofluids containing copper nanoparticles. A quantitative analysis of the velocity, temperature, and concentration profiles of the *Cu*-kerosene nanofluid is conducted for varying Pr and compared with different values of different dimensionless parameters.

The flow of an incompressible viscous fluid past a vertical plate is considered as an unsteady laminar natural convection boundary layer in two dimensions. The x-axis is vertically oriented upward along the axis of the plate. It is assumed that x is at the leading edge of the plate, where the thickness of the boundary layer is zero. The temperature and concentration of the stationary fluid around the origin is assumed to be at ambient temperature (T'_∞) and concentration (C'_∞) respectively. Initially it is

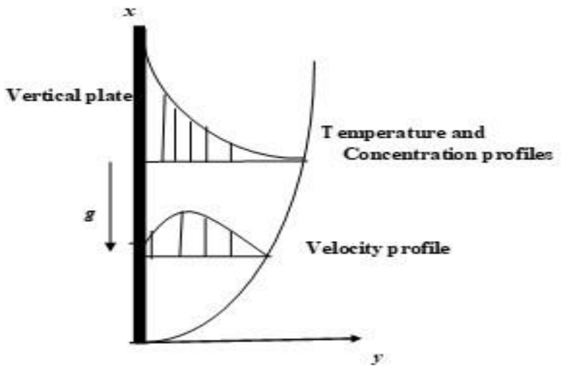

Figure 1. Geometry of fluid flow

assumed that the fluid and the plate are of the same temperature and concentration. When the time increases, the temperature of the plate is increased to T'_w and the concentration of the fluid near the plate is C'_w.

II. DESCRIPTION OF THE PROBLEM

Figure 1 depicts Geometry of fluid flow physically. Table 1 shows the thermophysical properties of kerosene and copper nanofluid. These assumptions lead to unsteady momentum, energy, and concentration equations for nanofluid that satisfy the Boussinesq approximation, as described by Tiwari and Das (2007).

$$\frac{\partial u}{\partial x}+\frac{\partial v}{\partial y}=0 \quad (1)$$

$$\frac{\partial u}{\partial t'}+u\frac{\partial u}{\partial x}+v\frac{\partial u}{\partial y}=\frac{1}{\rho_{nf}}\left[\mu_{nf}\frac{\partial^2 u}{\partial y^2}+(\rho\beta)_{nf}g(T'-T'_\infty)+(\rho\beta)^*{}_{nf}g(C'-C'_\infty)\right] \quad (2)$$

$$\left[\frac{\partial T'}{\partial t'}+u\frac{\partial T'}{\partial x}+v\frac{\partial T'}{\partial y}\right]=\left(\frac{(\rho C_p)_{nf}}{k_{nf}}\right)\left[\frac{\partial^2 T'}{\partial y^2}\right] \quad (3)$$

$$\frac{\partial C'}{\partial t'}+u\frac{\partial C'}{\partial x}+v\frac{\partial C'}{\partial y}=D\frac{\partial^2 C'}{\partial y^2} \quad (4)$$

*T*he initial and boundary conditions are

$$t'\le 0: u=0, v=0, T'=T'_\infty\ c'=c'_\infty \text{ for all } x \text{ and } y$$
$$t'>0: u=0, v=0, T'=T'_w\ c'=c'_w \text{ at } y=0$$
$$\text{At } x=0: u=0,\ v=0,\ T'=T'_\infty\ c'=c'_\infty$$
$$\text{At } y\to\infty:\ u\to 0,\ T'\to T'_\infty,\ c'\to c'_\infty \quad (5)$$

where *u* is the velocity along the *x*-axis, ρ_{nf},and μ_{nf}, are respectively, the effective density and effective dynamic viscosity of the nanofluid. Nanofluid thermal density is defined as β_{nf}, the chemical reaction coefficient is *R*, and the acceleration is determined by gravity. The nanofluid's thermal conductivity, K_{nf}. In order to determine the properties of nanofluid, we can follow the correlations shown below;

$$(\rho\beta)_{nf}-\varphi\rho_s=(1-\varphi)\rho_f$$
$$(\rho\beta)_{nf}-\varphi(\rho\beta)_s=(1-\varphi)(\rho\beta)_f$$
$$(\rho\beta)^*{}_{nf}-\varphi(\rho\beta)^*{}_s=(1-\varphi)(\rho\beta)^*{}_f$$
$$(\rho C_p)_{nf}-\varphi(\rho C_p)_s=(1-\varphi)(\rho C_p)_f \quad (6)$$

It is based on a model developed by Hamilton and Crossser (1962) is used to calculate effective thermal conductivity of nanofluids, which is as follows:

$$k_{nf}=k_s+(n-1)k_f-(n-1)\varphi(K_f-k_s) \quad (7)$$

$$k_f=k_s+(n-1)k_f+\varphi(K_f-k_s) \quad (8)$$

The spherical shape factor of nanoparticles is n. φ is solid volume fraction of nanoparticles, particularly spherical, $n = 3$ is defined. Nanofluid, base fluid, and solid nanofluid are represented by the subscripts nf, f, and s, which represent their thermophysical-chemical properties, respectively. Table 2 provides information on the thermal conductivity and dynamic viscosity of spherical-shaped nanoparticles.

A specific model can be removed from its quantitative features by rewriting its equation with dimensionless quantities. The number of parameters in qualitative studies can be reduced, allowing their comparison with previous literature to be more efficient. Discussions of physical values can take place with dimensionless quantities. Below are some measures of non-dimensionality:

$$X = \frac{x}{L}, \quad y = \frac{yGr^{\frac{1}{4}}}{L}, \quad U = \frac{uLGr^{\frac{-1}{2}}}{\upsilon_f}, \; V = \frac{vLGr^{\frac{-1}{4}}}{\upsilon_f}$$

$$t = \frac{t'\upsilon_f Gr^{\frac{1}{2}}}{L^2}, \; \theta = \frac{T' - T'_\infty}{T'_w - T'_\infty} \; \mu_{nf} = \frac{\mu_f}{(1-\varphi)^{2.5}}$$

$$c = \frac{c' - c'_\infty}{c'_w - c'_\infty} \;\; Sc = \frac{\upsilon_f}{D} \;\; \upsilon_f = \frac{\mu_f}{\rho_f}, \; ,\alpha_f = \frac{k_f}{(\rho C_p)_f}$$

$$Gm = \frac{g\beta^* L^3 (c_w - c_\infty)}{\upsilon_f^2} \;, Gr = \frac{g\beta L^3 (T_w - T_\infty)}{\upsilon_f^2}, \text{Pr} = \frac{\vartheta_f}{\alpha_f} \quad (9)$$

Thermal fluids have several characteristics, including the Grashof number(Gr), Prandtl number (Pr), In terms of kinematics (ϑ_f) the viscosity of the fluid and temperature diffusivity (α).A non-dimensional governing equation with a dimensionless initial condition and boundary conditions is described by

$$\frac{\partial U}{\partial X} + \frac{\partial V}{\partial Y} = 0 \quad (10)$$

$$\frac{\partial U}{\partial t} + U\frac{\partial U}{\partial X} + V\frac{\partial U}{\partial Y} = \frac{1}{(1-\varphi)^{2.5}} \frac{1}{\left(1-\varphi+\varphi\frac{\rho_s}{\rho_f}\right)} \frac{\partial^2 U}{\partial Y^2} + \left(\frac{1-\varphi+\varphi\frac{(\rho\beta)_s}{(\rho\beta)_f}}{1-\varphi+\varphi\frac{\rho_s}{\rho_f}}\right)\theta + \frac{Gm}{Gr}\left(\frac{1-\varphi+\varphi\frac{(\rho\beta)^*{}_s}{(\rho\beta)^*{}_f}}{1-\varphi+\varphi\frac{\rho_s}{\rho_f}}\right)C \quad (11)$$

$$\frac{\partial \theta}{\partial t} + U\frac{\partial \theta}{\partial X} + V\frac{\partial \theta}{\partial Y} = \frac{1}{\left(1-\varphi+\varphi\frac{(\rho C_p)_s}{(\rho C_p)_f}\right)} \frac{k_{nf}}{k_f Pr} \frac{\partial^2 \theta}{\partial Y^2} \quad (12)$$

$$\frac{\partial C}{\partial t} + U\frac{\partial C}{\partial X} + V\frac{\partial C}{\partial Y} = \frac{1}{Sc}\frac{\partial^2 C}{\partial Y^2} \quad (13)$$

$$\begin{gathered} t \le 0: U = 0, V = 0, T = 0 \;\; C = 0 \;\; \text{for all } X \text{ and } Y \\ t > 0: U = 0, V = 0, T = 1\,, C = 1 \;\; \text{at } X = 0 \\ Y = 0: \;\; U = 0, V = 0, T = 0 \;\; , C = 0 \\ Y \to \infty \;\to as\;\; U \to 0, T \to 0 \;\;\; C \to 0 \end{gathered} \quad (14)$$

$$\alpha_1 = \frac{1}{(1-\varphi)^{2.5}} \frac{1}{(1-\varphi+\varphi\frac{\rho_s}{\rho_f})}, \quad \alpha_2 = \left(\frac{1-\varphi+\varphi\frac{(\rho\beta)_s}{(\rho\beta)_f}}{1-\varphi+\varphi\frac{\rho_s}{\rho_f}}\right), \; \alpha_5 = \frac{1}{Sc}$$

$$\alpha_3 = \left(\frac{1-\varphi+\varphi\frac{(\rho\beta)^*{}_s}{(\rho\beta)^*{}_f}}{1-\varphi+\varphi\frac{\rho_s}{\rho_f}}\right), \alpha_4 = \frac{1}{\left(1-\varphi+\varphi\frac{(\rho C_p)_s}{(\rho C_p)_f}\right)} \frac{k_{nf}}{k_f Pr} \quad (15)$$

Now Eqs. (11), (12) and (13) in terms of α_1, α_2, $\alpha_3, \alpha_4, \alpha_5$ are

$$\frac{\partial U}{\partial X} + \frac{\partial V}{\partial Y} = 0 \quad (16)$$

$$\frac{\partial U}{\partial t} + U\frac{\partial U}{\partial X} + V\frac{\partial U}{\partial Y} = \alpha_1 \frac{\partial^2 U}{\partial Y^2} + \alpha_2 \theta + \alpha_3 \frac{Gm}{Gr} C \quad (17)$$

Table 1: Thermo physical properties of kerosene and Copper nanoparticles (Dash *et al.*, 2022):

Physical Properties	Kerosene /base fluid	Cu(copper)
$\rho\ (kg/m^3)$	783	8933
$C_p\ (J/kgK)$	2090	385
$K\ (W/m\ K)$	0.145	401
$\beta X10^{-5}(1/K)$	21	1.67
$\beta^* X10^{-6}\ (m^2/h)$	298.2	3.05

Table 2: Heat conductivity and the dynamic viscosity caused by the nanoparticles shape.

Shape of nano particles	Thermal conductivity	Dynamic Viscosity
Spherical	$\frac{k_{nf}}{k_f} = \frac{k_s + 2k_f - 2\varphi(k_f - k_s)}{k_s + 2k_f + \varphi(k_f - k_s)}$	$\mu_{nf} = \frac{\mu_f}{(1-\varphi)^{2.5}}$

$$\frac{\partial \theta}{\partial t} + U\frac{\partial \theta}{\partial X} + V\frac{\partial \theta}{\partial Y} = \alpha_4 \frac{\partial^2 \theta}{\partial Y^2} \quad (18)$$

$$\frac{\partial C}{\partial t} + U\frac{\partial C}{\partial X} + V\frac{\partial C}{\partial Y} = \alpha_5 \frac{\partial^2 C}{\partial Y^2} \quad (19)$$

The local and mean, Nusselt numbers, wall stress or skin friction coefficients, are calculated from the gradients of velocity and temperature, and in their non-dimensional form are as follows:

$$\tau_X = \frac{1}{(1-\varphi)^{2.5}} X\, Gr^{\frac{3}{4}} \left(\frac{\partial U}{\partial Y}\right)_{Y=0} \quad (20)$$

$$\bar{\tau} = \frac{1}{(1-\varphi)^{2.5}} Gr^{\frac{3}{4}} \int_0^1 \left(\frac{\partial U}{\partial Y}\right)_{Y=0} dX \quad (21)$$

$$Nu_X = -\frac{K_{nf}}{K_f} X \sqrt[4]{Gr} \left(\frac{\partial \theta}{\partial Y}\right)_{Y=0} \quad (22)$$

$$\overline{Nu} = -\frac{K_{nf}}{K_f} \sqrt[4]{Gr} \int_0^1 \left(\frac{\partial \theta}{\partial Y}\right)_{Y=0} dX \quad (23)$$

$$Sh_X = -X \sqrt[4]{Gr} \left(\frac{\partial C}{\partial Y}\right)_{Y=0} \quad (24)$$

$$\overline{Sh} = -\sqrt[4]{Gr} \int_0^1 \left(\frac{\partial C}{\partial Y}\right)_{Y=0} dX \quad (25)$$

III. ANALYSIS PROCEDURES FOR NUMERICAL DATA

The equations (17) - (19) is an expression for a nonlinear partial differential equation governed by the time-dependent initial and boundary conditions (14). Finite difference schemes based on Crank Nicolson discretization are used by Carnahan *et al*. (1969) in this method. This is accomplished by creating rectangular segments of the mesh comprised of $X_{max} = 1$and $Y_{max} = 16$ where Y_{max} corresponds to $Y = \infty$. A distance was calculated between a nodal point and a pivot point by considering the time step $\Delta t = 0.01$ and, the distance in the X and Y directions, respectively, with $\Delta X = 0.05$ and $\Delta Y = 0.2$. Validation of the implemented finite difference method is carried out in two step processes. In the first stage of validation ensures the accuracy of the scheme. In the second stage, the simulated results are validated with previous literature. The optimal grid-size (i.e., 100 X 500) which attains sufficient accuracy is chosen for the simulations mesh independent testing for the flow variables was used to check if the solution with the above mesh varied only in the third decimal place when increased by 50%. Truncation error is reduced to zero as mesh size ap-

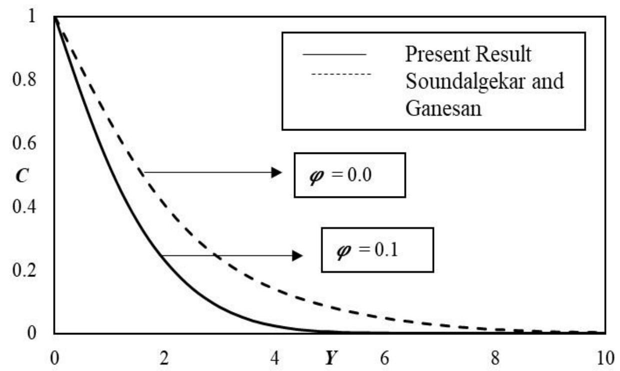

Figure 2. Comparison of concentration profile.

proaches zero. Therefore, this method is both stable and compatible, and it is also convergent.

IV. RESULTS AND DISCUSSION

A solution is given to the partial differential equation, and numerical expressions of velocity temperature and concentration, skin friction, Nusselt number, and Sherwood number are provided through visual illustrations of the thermal Grashof number (Gr), Prandtl number (Pr), and Schmidt number (Sc). As a result, the nanoparticles are considered to have a volume fraction of between $0 < \varphi < 0.2$. In the present study, Kerosene was used as the base fluid to analyze nanofluids containing copper (Cu) were analyzed. As a consequence, the flow phenomena are governed by the assumption of several pertinent parameters, and the characteristic of the numerical result is illustrated in Figs. 2-10, which demonstrate the influence of the following physical parameters: Pr (Prandtl number), Gr (Thermal Grashof number), Gm (Mass Grashof number), and Sc (Schmidt number) on velocity, temperature and concentration, skin friction Nusselt number and Sherwood number. The corresponding parameters $Pr = 23.0$, $Gr = 4.0$, $Gm = 2.0$, $Sc = 2.0$ are taken to be fixed in the simulation process is used to examine and study the behavior of the parameters.

Concentration transient plots provide a helpful benchmark against the previous, simpler models from the literature. It is possible to explain the flow of fluid past a plate without a nanofluid. This could be done using the earlier results (Soundalgekar and Ganesan, 1981) and by analyzing the accuracy of the Crank Nicolson computational code. A general conclusion from this study is that a model if $\varphi = 0.0$ is reduced to a flow model. This is the same as the model reported in Soundalgekar and Ganesan (1981). The simulation of the transient concentration profile ($t = 4.1500$) for $Pr = 0.73$, $Sc = 0.78$ in Fig. 2 indicates that our results are very close to those Soundalgekar and Ganesan (1981).

Figure 3 illustrates the effect of Pr, Gr, Gm and φ values on the velocity profile of Cu-kerosene based nanofluid. A thermal diffusivity number of Pr characterizes the relationship between viscosity and thermal diffusivity.

More heat can be transferred from the plate to the fluid by extending the duration of the process. The diffusion of heat is enhanced with a lower Prandtl number.

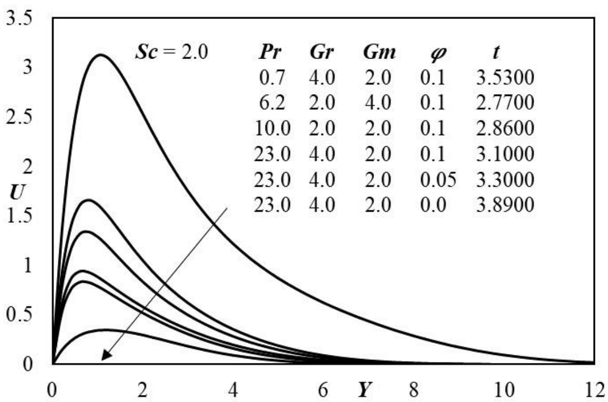

Figure 3. The impact of Pr, Gr, Gm and φ values on Velocity profile.

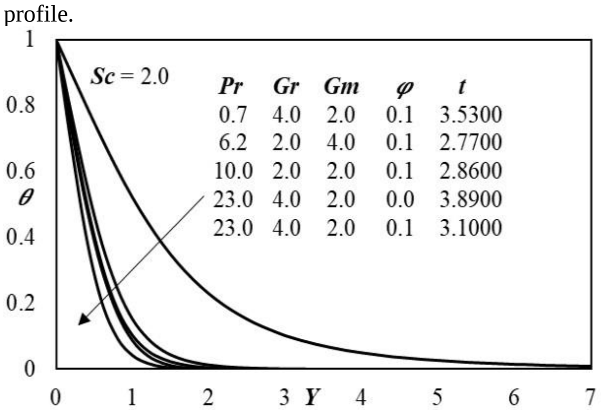

Figure 4. The impact of Pr, Gr, Gm and φ values on Temperature profile.

The temperature and buoyancy of the fluid both increase, resulting in a rise in velocity. Distribution of velocity is also facilitated by the concentration difference. The increase in Gc and Gr increases buoyancy forces, which increases fluid velocity. Furthermore, the velocity decreases and Gr and Gm increase along with this flow pattern. The velocity peaks close to the vertical plate. Nevertheless, it decays as the distance from the vertical plate increases until it can meet the free stream requirement. As a result of this analysis, the importance of mass and heat diffusion becomes apparent. It is observed that the time taken to reach the steady state increases with increasing value of Pr. The velocity decreased as the nano volume fraction increased. An increase in nano volume fraction leads to an increase in the thickness of the momentum boundary layer. The reason for this is that copper has a higher thermal conductivity than other fluids. This is caused by an increase in nanoparticle concentration, which increases the viscosity of the particle suspension.

Figure 4 shows the effect of Pr, Gr, and Gm values on the temperature profile of Cu-kerosene-based nanofluid. Convection occurs when a heavier molecule lifts a lighter molecule. This lift is associated with an increase in velocity due to the Prandtl number (Pr). Temperature differences between heavier and lighter molecules cause this lift. The thermal Grashof number (Gr) is a measure of the thermal conductivity of the plate, which lowers the temperature near the wall. Due to the mass Grashof number (Gm) inclusion of nanoparticles, the so-

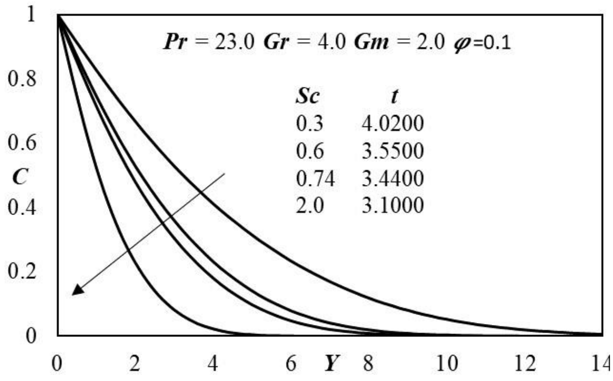

Figure 5. The impact of Sc values on Concentration profile.

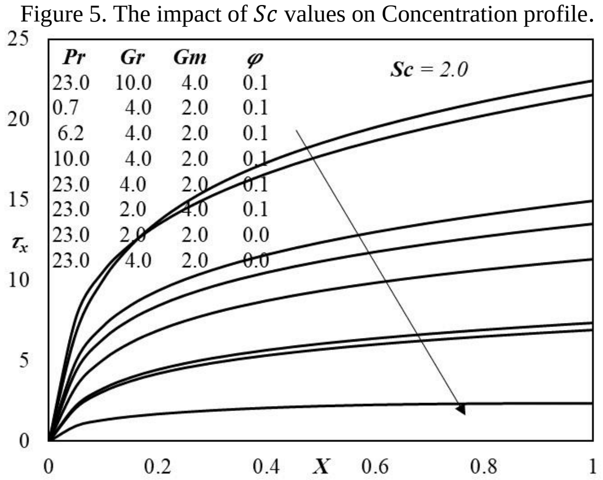

Figure 6. Local skin friction $\boldsymbol{\tau_x}$

lutal buoyancy decreases due to the concentration difference between the wall and air, lowering the temperature profile. The characteristics of the nano volume fraction on fluid temperature are shown in the same figure. The heat conductivity of a metal is an important consideration when choosing a metal for a specific application. The excellent conductivity of copper makes it an ideal material for heat transfer. The combined effect of the base fluid and copper nanoparticles was increased by increasing the volume fraction. Fluid temperatures rise when the fluid velocity is slowed by the higher particle density in any domain.

Figure 5 highlights the impact of the Schmidt number on the concentration profile. As the Schmidt number is increased, and the concentration profile diminishes. Consequently, it is affected by the thickness of the mass transfer boundary layer resulting from a velocity boundary layer. Species present in the atmosphere are represented by Sc. A decrease in viscosity is accompanied by an increase in the Schmidt number when species diffusion occurs. A fall in the transport phenomenon appears as well. Diffusion rates tend to decrease as the Schmidt number increases. Higher values of the Schmidt number cause a diminution in the concentration profile.

For different values of Pr, Gr, Gm, and Sc, Figure 6 illustrates the effects of local skin friction coefficient profiles. Shear stress is related to the coefficient of skin friction, which explains fluid movement. Natural convection over the plate gives rise to heat transfer. The heat exchange occurs when frictional forces are created. It is ob-

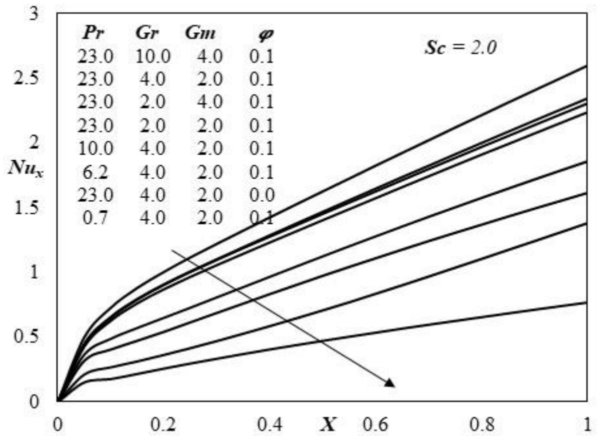

Figure 7. Local Nusselt number Nu_x

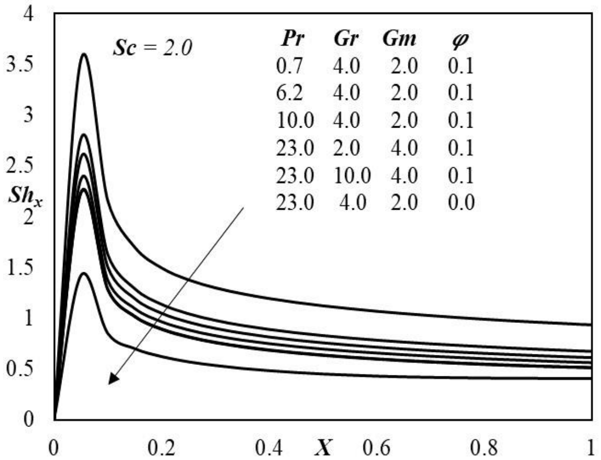

Figure 8. Local Sherwood number Sh_x

served that velocity indicates the level of shear stress which increases the local skin friction. Figure 7 shows local Nusselt numbers in combination with of Pr, Gr, Gm, and Sc parameters. The Nusselt number is a dimensionless parameter that indicates the proportion of heat transferred by convection to conduction in the fluid.

This number describes a temperature gradient. When Gr and Gc become greater, heat is transferred at a faster rate. Nanoparticles in a fluid increase the viscosity of the fluid due to the temperature difference, which in turn increases the local Nusselt number profile. Figure 8 shows the effect of local Sherwood numbers, considering Pr, Gr, Gm, and Sc. The dimensionless Sherwood number plays a vital role in the mass transport and energy involved with fluid flow. Sherwood number represents the correlation between convective mass transfer and diffuse mass transfer. Nanoparticles are involved in the transport process of momentum during convection near the plate, the local Sherwood number increases, and it declines towards the wall. Nanoparticles influence average skin friction according to governing parameters Pr, Gr, Gm, and Sc are shown in Fig. 9. Shear stress, results in an increase in the thickness of the boundary layer. A mean fluid velocity can be calculated if a flow is moving over a plate combined with other physical parameters. As the mean fluid velocity increases, the average friction increases as well. Figure 10 illustrates the average Nusselt number

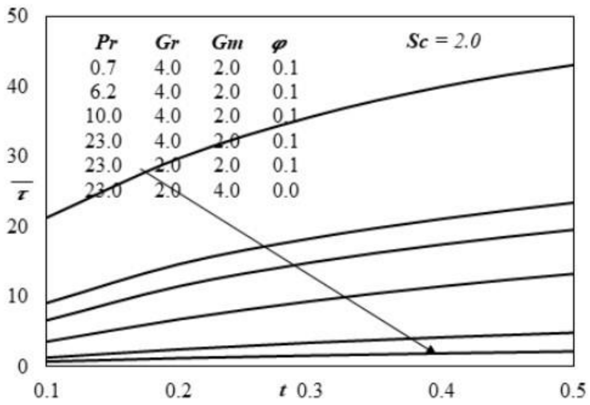

Figure 9. Average skin friction $\bar{\tau}$

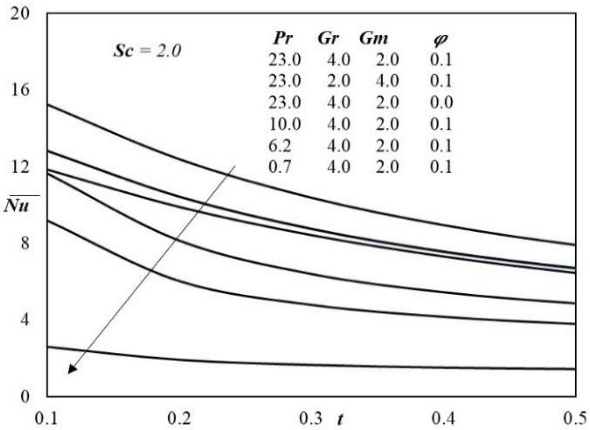

Figure.10. Average Nusselt number $\overline{Nu}$

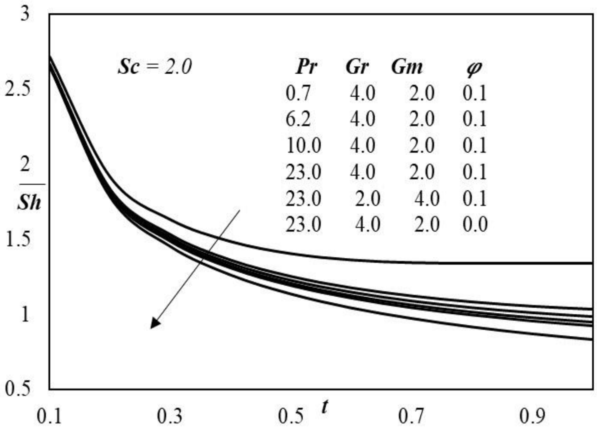

Figure 11. Average Sherwood number $\overline{Sh}$

profile due to the presence of dominant parameters Pr, Gr, Gm, and Sc. The average Nusselt number is the sum of all the local Nusselt numbers across the entire heat transfer surface. The heat transfer coefficient decreases with an increase in nano particle concentration observed.

Figure 11 depicts convection-induced diffusion measured by the average Sherwood number. Mass transfer by convection occurs when material moves between a surface and a moving fluid. Mass transfer coefficients are affected by fluid characteristics. The driving force is determined by the concentration difference between the fluid and the boundary. Sherwood number profiles are significantly lower when the mass transfer coefficient decreases.

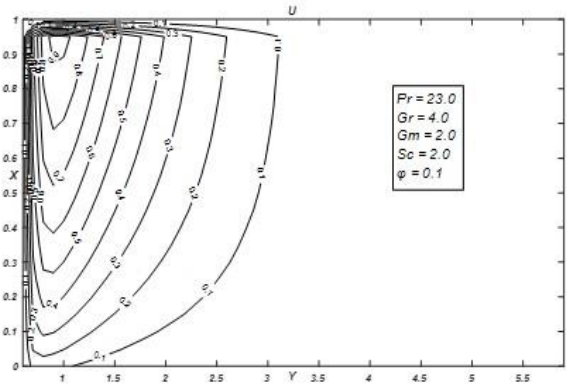

Figure 12. Plots of Velocity contours

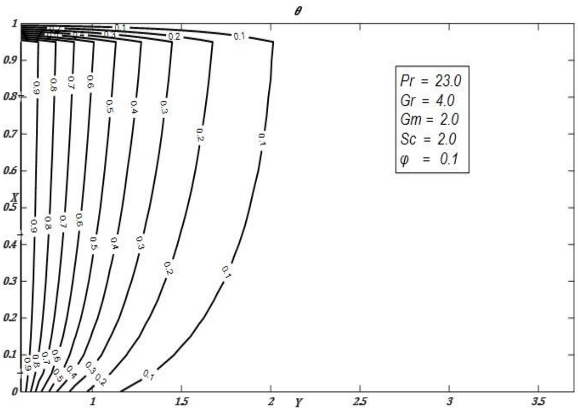

Figure 13. Plots of Temperature contours.

The velocity, temperature, and concentration of fluid properties are plotted using contour plots. Figures 12-14 illustrate the three-dimensional cross-section representing contour lines for the values of the Prandtl number ($Pr = 23.0$), thermal Grashof number ($Gr = 4.0$), mass Grashof number ($Gm = 2.0$), and Schmidt number ($Sc = 2.0$) and volume fraction ($\varphi = 0.1$) . An analysis of the velocity contour plot for kerosene-based nanofluid is depicted in Fig. 12. Lines representing equal heights are presented as contours. The dispersion of contour curves increases with the Prandtl number. The constant values of a scalar property are known as isocontour plots. Figure 13 illustrates the temperature contour plots of the kerosene-based nanofluid. Flow properties are quickly identified by a contour plot by identifying regions with high or low temperatures. The labeled values indicate that the temperature rises near the plate due to its heat transfer rate. The density of data points is shown by contour plots. Graphs of three-dimensional functions are plotted as contour plots. Contour boundaries are isolines with constant densities.

According to Fig. 14, a small variation in mass transport has an impact on kerosene-based nanofluids.

The present study provides a foundation for future research on kerosene-based nanofluids. In addition to laminar flow on plates, cones and cylinders, discussion can be extended to turbulent flow. Due to various industrial applications, the results demonstrate the possibility of in-

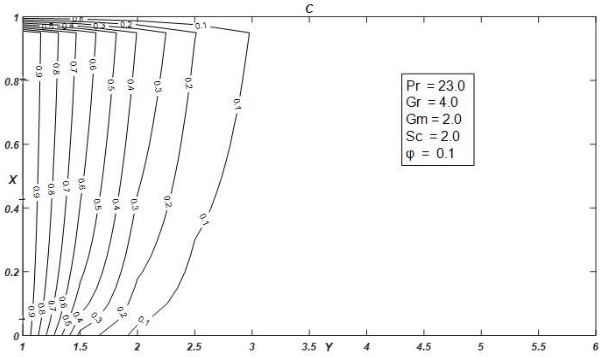

Figure 14. Plots of Concentration contours

creasing mass and thermal energy transport using nanoparticles about the fundamental characteristics of kerosene. Moving boundaries can also be included in the mathematical model.

V. CONCLUSIONS

A study of the flow of a nanofluid over a vertical plate with uniform velocity is presented using an implicit finite difference method known as the Crank-Nicholson method for elucidating the results graphically. The following was our impression:

1. Prandtl numbers show noticeable changes in velocity distribution. The velocity boundary layer thickness is generally reduced and the thermal boundary layer thickness is increased with increasing Pr values.
2. Thermal boundary layers evolve faster than velocity boundary layers. Nanoparticles improve the thermal conductivity of the base fluid.
3. The thermal Grashof number increases buoyancy forces. The enhancement of thermal conductivity also increases the convective heat transfer rate when the Pr value is high.
4. Mass transport of Copper nanoparticles enhances mass transfer and increases convective heat transfer coefficients by increasing the value of Gc and Sc, thereby decreasing the concentration profile.
5. Fluids with a high viscosity transfer heat more efficiently than fluids with a low viscosity. When the Grashof number (Gr) and the Grashof number (Gc) are lower, Pr steadily rises.

REFERENCES

Acharya, N., Das, K. and Kundu, P.K. (2016) The squeezing flow of Cu-water and Cu – kerosene nanofluids between two parallel plates. *Alexandria Engineering Journal*. **55**, 1177–1186.

Bhatti, M.M, Doranehgard, M.H and Ellahi, R. (2022) Electro-magneto-hydrodynamic Eyring-Powell fluid flow through micro-parallel plates with heat transfer and non-Darcian effects. *Math. Meth. Appl. Sci*. 1-15. doi:10.1002/mma.8429

Bhatti, M.M, Beg, O.A., Ellahi, R. and Abbas, T. (2022) Natural Convection Non-Newtonian EMHD Dissipative flow through a Microchannel containing a Non-Darcy porous Medium: Homotopy Perturbation Method study. *Qual. Theory Dyn Syst*. **21**, 97.

Daniel, Y.S., Usman, A. and Haruna, U. (2022) Effect of Electric Field Flow on Nanofluid over Stretchable Surface. *Science World Journal*. **17**, 186-190.

Dash, R.K., Mishra, S.R. and Pattnaik, P.K. (2022) Influence of Radiative Heat Energy on the MHD Flow of Cu-kerosene Nanofluid Over a Vertical Plate: Laplace Transform Technique. *Biointerface Research in Applied Chemistry*. **12**, 6234 – 6251.

Hamilton, R.L. and Crosser, O.K. (1962) Thermal Conductivity of Heterogeneous Two-Component Systems. *I & EC Fundamental*. **1,** 187-191.

Hassani, M., Mohammad Tabar, M., Nemati, H., Domairry, G. and Noori, F. (2011) An analytical solution for boundary layer flow of a nanofluid past a stretching sheet. *International journal of thermal Sciences*. **50**, 2256-2263.

Ishak, A., Yacob, N.A. and Bachok, N. (2011) Radiation effects on the thermal boundary layer flow over a moving plate with convective boundary condition. *Meccanica*. **46**, 795-801.

Kasaeian, A., Daneshazarian, R., Mahian, O., Kolsi, L., Chamkha, A.J., Wongwises, S. and Pop. L. (2017) Nanofluid flow and heat transfer in porous media: A review of the latest developments. *Int. Journal of Heat and Mass Transfer*. **107**, 778-791.

Khan, W.A. and Pop, I. (2010) Boundary-layer flow of a nanofluid past a stretching sheet. *International Journal of Heat and Mass Transfer*. **53**, 2477-2483.

Mutuku-Njane, W.N. and Makinde, O.D. (2014) MHD Nanofluid Flow Over a Permeable Vertical Plate with Convective Heating. *Journal of Computational and Theoretical Nanoscience*. **11**, 667–675.

Narayana, P.V., Satya Akshit, S., Ghori Jatin, P. and Venkatesearlu, B. (2017) Thermal radiation effects on an unsteady MHD nanofluid flow over a stretching sheet with non-uniform heat source/sink. *Journal of Nanofluids*. **6**, 899-907.

Nield, D.A. and Kuznetsov, A.V. (2009) Thermal instability in a porous medium layer saturated by nanofluid. *International journal of Heat and Mass Transfer*. **52**, 5796-5801.

Noghrehabadi, A., Ghalambaz, M. and Ghanbarzadeh, A. (2014) Effects of variable viscosity and Thermal conductivity on natural convection of nanofluids past a vertical plate in porous media. *Journal of Mechanics.* **30**, 265- 275.

Rashidi, M.M., Mahariq, I Alhuyi Nazari, M., Accouche, O. and Bhatti, M.M. (2022) Comprehensive review on exergy analysis of shell and tube heat exchangers. *J. Therm. Anal. Calorim*. **147**, 12301-12311.

Reddy, Y.D., Ramya, D. and Babu, L.A. (2016) Effect of thermal radiation on MHD boundary layer flow of nanofluid and heat transfer over a non-linearly stretching sheet with transpiration. *Journal of Nanofluids.* **5**, 889-897.

Saritha, K. and Palaniammal, S. (2018) MHD viscous nanofluid flow with base fluids' water and kerosene in the presence of a temperature gradient dependent heat sink with prescribed heat flux. *Latin American Applied Research.* **48**,139-144.

Sobamowo, M.G. (2019) Free convection flow and heat transfer of nanofluids of different shapes of nano-sized particles over a vertical plate at low and high Prandtl numbers. *J. Appl. Comput. Mech.* **5,** 13-39.

Soundalgekar, V.M. and Ganesan, P. (1981) Finite difference analysis of transient free convection with mass transfer on an Isothermal vertical flat plate. *Int. J. Engg. Sci.* **19**, 757-770.

Tiwari, R.K. and Das, M.K. (2007) Heat transfer augmentation in a two-sided lid-driven differentially heated square cavity utilizing nanofluids. *International Journal of Heat and Mass Transfer*. **50**, 2002-2018.

Carnahan, B., Luther, H.A. and Wilkes, J.O. (1969) *Applied Numerical Methods*, John Wiley and Sons, New York.

Received: March 3, 2022
Sent to Subject Editor: April 7, 2022
Accepted: December 19, 2022
Recommended by Subject Editor Fabio Giannetti